Letter

Mechanics of cup-shaped caveolae

Ahis Shrestha [1], Fabien Pinaud [2], and Christoph A. Haselwandter [1]

[1] *Department of Physics and Astronomy and Department of Quantitative and Computational Biology, University of Southern California, Los Angeles, California 90089, USA*

[2] *Department of Biological Sciences, Department of Physics and Astronomy, and Department of Chemistry, University of Southern California, Los Angeles, California 90089, USA*

(Received 20 January 2021; accepted 16 July 2021; published 6 August 2021)

Caveolae are cell membrane invaginations of defined lipid and protein composition that flatten with increasing membrane tension. Super-resolution light microscopy and electron microscopy have revealed that caveolae can take a variety of cuplike shapes. We show here that, for the range in membrane tension relevant for cell membranes, the competition between membrane tension and membrane bending yields caveolae with cuplike shapes similar to those observed experimentally. We find that the caveola shape and its sensitivity to changes in membrane tension can depend strongly on the caveola spontaneous curvature and on the size of caveola domains. Our results suggest that heterogeneity in caveola shape produces a staggered response of caveolae to mechanical perturbations of the cell membrane, which may facilitate regulation of membrane tension over the wide range of scales thought to be relevant for cell membranes.

DOI: 10.1103/PhysRevE.104.L022401

I. INTRODUCTION

Caveolae are small membrane invaginations with a size of the order of 100 nm that are enriched in caveolin-1 proteins as well as a number of other proteins and lipids [1,2]. Caveolae are highly abundant in the plasma membranes of certain mammalian cell types, such as muscle and endothelial cells, in which they can encompass half of the total membrane area [2,3]. Caveolae respond to changes in membrane tension by altering their curved shape [1–6]. In particular, caveolae flatten out and, ultimately, (partially) disassemble in response to cell swelling and cell stretching, and thereby provide a reservoir of (in-plane) membrane area and a buffer against changes in membrane tension [5,7,8]. Caveolae are thought to have biologically important roles in mechanosensing, mechanotransduction, membrane area and membrane tension homeostasis, plasma membrane organization and signaling, and lipid regulation [1–3,6,9,10].

Super-resolution light microscopy (SRM) and electron microscopy (EM) experiments have demonstrated that caveolae can take a variety of cuplike shapes resembling spherical caps [1,2,10–16]. For instance, three-dimensional super-resolution fluorescence imaging of caveolin-1 in mouse embryonic fibroblast cells [14] shows that caveolae can take cuplike shapes with variable invagination depths, areas, and radii of curvature (see Fig. 1). Motivated by these experimental observations, we employ here the theoretical framework developed in Ref. [17] to study the mechanics of cup-shaped caveolae. Previously it was found [5,18] that the competition between membrane tension and line tension along the caveola domain boundary yields fully flattened or fully budded (spherical) caveola shapes. We show here that, as the membrane tension is changed, the preferred spontaneous curvature of caveola domains can yield a continuous spectrum of cuplike caveola shapes intermediate between fully flattened and fully budded caveola states. For the range in membrane tension relevant for cell membranes and the spontaneous curvature associated with caveola domains, our calculations predict that caveolae adopt cuplike shapes similar to those observed experimentally [1,2,10–16] [Fig. 1(a)]. We find that the caveola shape and its response to changes in membrane tension can depend strongly on the caveola spontaneous curvature and on the size of caveola domains. Our calculations suggest that caveolae show a staggered response to changes in membrane tension, which may facilitate regulation of membrane tension over the wide range of scales thought to be relevant for cell membranes [19–21].

II. CAVEOLA ENERGY

Based on SRM and EM observations [1,2,10–16] and previous theoretical models [5,18,25] we describe caveolae as membrane domains that take the shape of spherical caps [24] with radius of curvature R and fixed surface area $S = \pi L^2$, where L is the in-plane radius of the flattened caveola (Fig. 1). While the assumption of a fixed caveola area is consistent with experiments showing that the number of caveolin-1 proteins in curved caveolae is approximately constant with only a small pool of caveolin-1 outside caveolae [26,27], we also note that flattened caveolae may disassemble [7], which may provide a mechanism for plasticity in caveola size. The caveola shape is conveniently specified by the fraction of the surface of a sphere of radius R covered by the caveola, $\beta = L^2/4R^2$, with $\beta = 0$ for completely flattened caveolae, $\beta = 1$ for fully budded caveolae, and $0 < \beta < 1$ for intermediate caveola states taking the shape of spherical caps or cups [Fig. 1(b)].

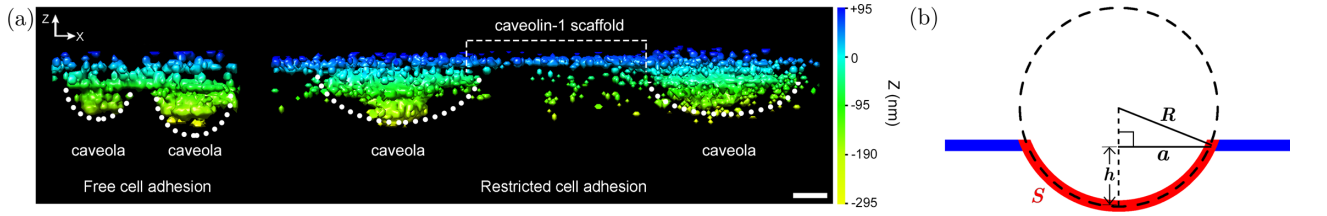

FIG. 1. Cup-shaped caveolae. (a) Two-dimensional z-x rendering of caveolae obtained from three-dimensional super-resolution fluorescence imaging of caveolin-1 at the plasma membrane for mouse embryonic fibroblast cells freely adhering to fibronectin substrates (left) and with adhesion constrained to 210×10 μm^2 fibronectin islands (right). Changes in the cell adhesion geometry are expected to modify the cell adhesion forces [22,23], and the shape and organization of caveolae [14]. The white dotted curves indicate the approximate position of the plasma membrane for the observed caveolae. Scale bar: 100 nm (adapted with permission from Ref. [14]). (b) Schematic of the spherical cap model of caveola shape, with the caveola domain indicated in red and the surrounding membrane indicated in blue. We denote the caveola surface area by $S = \pi L^2$, the caveola radius of curvature by R, the caveola base radius by a, and the caveola invagination depth by h [24].

Caveola membrane domains have an approximate size within the range $50 \lessapprox L \lessapprox 100$ nm [1,2,10–16]. In agreement with SRM and EM observations [1,2,10–16], these lower and upper bounds on L yield 25 nm $\lessapprox R < \infty$ and 50 nm $\lessapprox R < \infty$ for $0 < \beta \lessapprox 1$, respectively [Fig. 1(a)].

We consider three additive contributions to the caveola energy G that depend on caveola shape. First, the caveola energy involves a contribution $G_\sigma = 2\pi\sigma a$, where σ is the line tension along the caveola domain boundary and the in-plane caveola base radius $a = L\sqrt{1-\beta}$ [Fig. 1(b)]. Nonzero σ can arise, for instance, from differences in molecular composition between caveola domains and the surrounding membrane [17,28]. Previous work on lipid domain formation in bilayer membranes [17,28] suggests $0 \lessapprox \sigma \lessapprox 1\ k_BT$/nm. Interactions between caveolae and the surrounding membrane may also yield an effective contribution to the line tension that depends on caveola shape. We take here a phenomenological approach and consider, on the one hand, the constant values $\sigma = 0$ and $1\ k_BT$/nm. On the other hand, to explore how a dependence of σ on β may affect caveola shape, we also permit σ to linearly increase or decrease with β. The latter two scenarios correspond to situations in which the composition of the membrane surrounding caveolae favors flat or curved membrane shapes, respectively. In general, $\sigma(\beta)$ may also depend explicitly on membrane mechanical properties such as membrane tension.

Second, the caveola energy involves a contribution G_κ describing the energy cost of bending caveolae away from their preferred shape. For the spherical cap geometry of caveolae, the Helfrich-Canham-Evans membrane bending energy [29–31] yields

$$G_\kappa = \tfrac{1}{2}\kappa S(C - C_0)^2, \tag{1}$$

where κ is the membrane bending rigidity, $C = 2/R$ is the sum of the two principal curvatures of caveolae [Fig. 1(b)], and C_0 is the caveola spontaneous curvature. We use the value $\kappa = 20\ k_BT$ [19] for all the calculations described here. Caveolae are enriched in the curvature-generating integral membrane protein caveolin-1 [1,2] that, in a model bacterial system such as *E. coli*, can generate vesicles with the size and caveolin-1 composition of budded caveolae [32]. These observations suggest that the unperturbed state of caveolae is curved and, hence, $C_0 \neq 0$ in Eq. (1). EM observations of budded caveolae [1,2,10–13,33] indicate $0.04 \lessapprox C_0 \lessapprox 0.08$ nm^{-1}. For completeness, we also consider here the special case $C_0 = 0$ in Eq. (1). In addition to the contribution in Eq. (1) due to the mean curvature, the caveola membrane bending energy may, in general, also include a Gaussian curvature term [30], which would give rise to a boundary term evaluated along the caveola perimeter [34]. This term is identical to zero if the Gaussian membrane bending rigidities inside and outside caveolae are equal to each other. If there is a substantial difference in the Gaussian membrane bending rigidities inside and outside caveolae, the Gaussian boundary term could be included in the model described here as an additional, β-dependent contribution to the effective caveola line tension [34]. We do not explicitly consider here effects due to the Gaussian membrane curvature.

Third, the caveola energy involves a contribution $G_\gamma = \gamma(S - \pi a^2)$ corresponding to the work required to form a curved caveola shape against a (lateral) membrane tension γ. The value of γ strongly depends on the cell type and on the cell state, as well as on the location within the cell membrane [21]. Roughly, one expects that $10^{-4} \lessapprox \gamma \lessapprox 1\ k_BT$/nm^2 [19,20]. For buds forming in membranes with no area reservoirs, which can be the case for some bacterial cell types, one generally needs to consider a contribution to the bud energy due to membrane stretching, which would be proportional to the square of the fractional change in membrane area [35]. For the mammalian cell types of principal relevance for caveolae, however, the available membrane area can readily change without membrane stretching [36,37], and we therefore do not include the energy cost of membrane stretching in the caveola energy.

The total caveola energy $G = G_\sigma + G_\kappa + G_\gamma$ can thus be expressed as a function of the caveola shape parameter β in the form

$$G = 2\pi L\sigma(\beta)\sqrt{1-\beta} + 8\pi\kappa\left(\sqrt{\beta} - \frac{LC_0}{4}\right)^2 + \pi L^2\gamma\beta. \tag{2}$$

We minimize the caveola energy G in Eq. (2) with respect to β to determine the stable (energetically most favorable) caveola shapes $\beta_{\min}$ as a function of membrane tension for the parameter ranges of L, σ, and C_0 relevant for caveolae. Minimization of G in Eq. (2) amounts to solving a linear equation for $\sigma = 0$ and a quartic equation for a constant $\sigma > 0$, permitting exact analytic solutions. However, for the scenarios with a (linear) dependence of σ on β considered

here, minimization of Eq. (2) leads to a polynomial equation of degree greater than 4, in which case an analytic solution is not feasible [38]. To treat all the choices for σ considered here on the same footing, we numerically determine $\beta_{\min}$ throughout this Letter by minimizing G in Eq. (2) using the NUMPY.ARGMIN function implemented in the NUMPY package of the programming language PYTHON (version 2.7.12). We checked our numerical solution procedure against the exact analytic solutions available for constant σ.

For constant σ and $\gamma = 0$, the caveola energy in Eq. (2) reduces to the energy studied in Ref. [17] in the context of membrane budding driven by line tension. For constant σ and $C_0 = 0$, Eq. (2) reduces to the energy introduced in Ref. [5] to describe bistable caveolae with $\beta \approx 0$ or 1. An energy similar to Eq. (2) with constant σ was also recently employed [18] in the context of a two-state model of caveolae with $\beta \approx 0$ or 1. We show here that, for the values of γ, L, σ, and C_0 relevant for caveolae in cell membranes, Eq. (2) can yield stable cuplike caveola shapes with $0 < \beta < 1$ similar to those observed experimentally [1,2,10–16] [Fig. 1(a)]. We do not consider in Eq. (2) possible contributions to the caveola energy due to nematic ordering of lipids or proteins in caveolae [39]. In addition to caveola-induced membrane shape deformations [25], such contributions to the caveola energy may affect the formation of caveola clusters or produce more complicated caveola shapes deviating from the spherical cap geometry we focus on here. Furthermore, caveolae may interact with the cytoskeleton [11], resulting in the exertion of forces on caveolae. Such interactions may modify the mechanical properties of caveolae by, for instance, coupling curvature-sensing or curvature-inducing proteins in caveolae with the cytoskeleton, or penalizing shear deformations of caveolae [40–43]. Finally we note that, while we focus here on the interplay between cuplike caveola shapes and membrane tension, cup-shaped membrane buds can form even in the absence of membrane tension through area differences between the outer and inner membrane leaflets [44].

III. STABLE CAVEOLA SHAPES FOR $\gamma > 0$

It was found previously [17] that, for $\gamma = 0$, a nonzero line tension in Eq. (2) can yield stable membrane bud shapes with $0 < \beta < 1$. We find here that, for $\gamma > 0$, Eq. (2) yields stable cuplike caveola shapes with $0 < \beta < 1$ similar to those observed experimentally [1,2,10–16], even if $\sigma = 0$ [see the solid curves in Fig. 2]. In particular, at small membrane tension with $\sigma = 0$, Eq. (2) predicts stable caveola shapes with $\beta \gtrapprox 0.4$ and a shallow minimum in G. As the membrane tension is increased, the minimum in G becomes more sharply defined and $\beta_{\min}$ shifts smoothly towards $\beta_{\min} = 0$. In contrast, for $\sigma = 1\ k_BT/\text{nm}$ in Fig. 2 we find a discontinuous transition from fully budded caveolae with $\beta \approx 1$ to partially flattened caveolae with $\beta \approx 0.2$ at a critical membrane tension $\gamma^* \approx 0.028\ k_BT/\text{nm}^2$ (see the dashed curves in Fig. 2). It is instructive to compare these results to previous work on caveolae [5], which showed that a constant σ and $C_0 = 0$ in Eq. (2) yield a discontinuous transition in caveola shape, from fully budded ($\beta \approx 1$) to flattened ($\beta \approx 0$) caveola states without any stable intermediate states. Figure 2 thus suggests

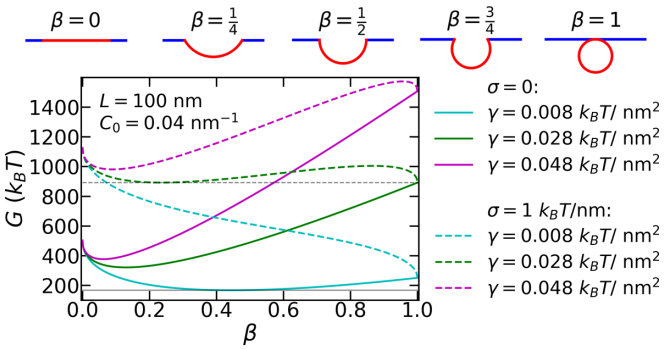

FIG. 2. Caveola energy G in Eq. (2) as a function of the caveola shape parameter β for $\gamma = 0.008$, 0.028, and 0.048 k_BT/nm^2 with $\sigma = 0$ (solid curves) and $\sigma = 1\ k_BT/\text{nm}$ (dashed curves). The solid and dashed horizontal lines indicate the energy minima of the cyan solid and green dashed curves, respectively. We set $L = 100$ nm and $C_0 = 0.04\ \text{nm}^{-1}$. The schematics in the top panels show caveolae (indicated in red) with shape parameters $\beta = 0$, 1/4, 1/2, 3/4, and 1 (left to right). We set $\kappa = 20\ k_BT$.

that cup-shaped caveolae are stabilized by the competition between membrane tension and membrane bending with $C_0 \neq 0$.

To further characterize the cuplike caveola shapes in Fig. 2 we note that, for $\sigma = 0$, G in Eq. (2) has a unique minimum at

$$\beta_{\min} = \min\left(1, \left[\frac{2\kappa L C_0}{8\kappa + L^2\gamma}\right]^2\right). \tag{3}$$

The solid curves in Fig. 3(a) show $\beta_{\min}$ with $\sigma = 0$ as a function of γ for $L = 50$ and 100 nm. First note that we always have $\beta_{\min} = 0$ for $C_0 = 0$ in Fig. 3(a) because G linearly increases with β for $C_0 = 0$ and $\sigma = 0$. In this hypothetical scenario, flattened caveola shapes provide the minimum-energy caveola states for any value of the membrane tension. Conversely, Fig. 3(a) shows that, for $C_0 \neq 0$ and $\sigma = 0$, Eq. (2) can yield stable caveola shapes with any β within the range $0 \leqslant \beta \leqslant 1$, with different $\beta_{\min}(\gamma)$ for different C_0 and L. Equation (3) and Figs. 2 and 3(a) show that the sequence of minimum-energy caveola shapes as a function of membrane tension depends crucially on C_0 and L, which may take different values for different caveolae.

In particular, at zero membrane tension, caveolae with $\sigma = 0$ in Fig. 3(a) are in their most budded state $\beta^0_{\min} = \min(1, [LC_0/4]^2)$. As the membrane tension is increased, one obtains stable caveola shapes with $0 \leqslant \beta < \beta^0_{\min}$ for $\sigma = 0$. Provided that $L \geqslant 4/C_0$, variations in membrane tension within the range relevant for cell membranes [19–21] thus yield, for $\sigma = 0$, the entire spectrum of stable caveola shapes, $0 \lessapprox \beta_{\min} \lessapprox 1$. This scenario is illustrated in Fig. 3(a) for $C_0 = 0.08\ \text{nm}^{-1}$ with $L = 50$ nm, and for $C_0 = 0.04$ and $0.08\ \text{nm}^{-1}$ with $L = 100$ nm, respectively. In this regime, caveolae have a constant $\beta_{\min} = 1$ for $\gamma \leqslant \overline{\gamma}$, where the threshold membrane tension $\overline{\gamma}$ is given by

$$\overline{\gamma} = \frac{2\kappa}{L^2}(LC_0 - 4). \tag{4}$$

Fully budded caveola shapes are stable if $\gamma \leqslant \overline{\gamma}$ and are gradually flattened as the membrane tension is increased beyond

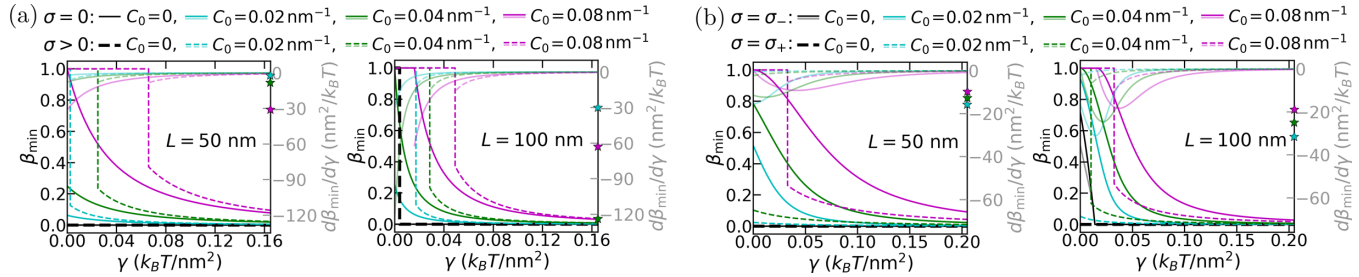

FIG. 3. Global minimum of G in Eq. (2) within the range $0 \leqslant \beta \leqslant 1$, $\beta_{\min}$ (left axes and opaque curves) and corresponding derivative of $\beta_{\min}$ with respect to membrane tension, $d\beta_{\min}/d\gamma$, for $0 < \beta_{\min} < 1$ (right axes and partially transparent curves) as a function of membrane tension γ for (a) $\sigma = 0$ (solid curves) and $\sigma > 0$ with $\sigma = 1\ k_BT/\text{nm}$ (dashed curves) and for (b) $\sigma = \sigma_-(\beta) = (1-\beta)\ k_BT/\text{nm}$ (solid curves) and $\sigma_+(\beta) = \beta\ k_BT/\text{nm}$ (dashed curves) using $C_0 = 0$, 0.02, 0.04, 0.06, and 0.08 nm^{-1} at $L = 50$ nm (left panels) and $L = 100$ nm (right panels). We use the same labeling scheme for $\beta_{\min}$ and $d\beta_{\min}/d\gamma$. The stars along the right axes mark the maximum magnitudes of $d\beta_{\min}/d\gamma$ and $\mathcal{S}_{\max}$, for the $\sigma = 0$ and σ_- curves, using the same color scheme as for the $d\beta_{\min}/d\gamma$ curves. We set $\kappa = 20\ k_BT$.

$\gamma = \overline{\gamma}$. For instance, for $L = 100$ nm and $C_0 = 0.08\ \text{nm}^{-1}$ we have $\overline{\gamma} = 0.016\ k_BT/\text{nm}^2$ [see the purple solid curve in the right panel of Fig. 3(a)]. For $\sigma = 0$ and $\gamma \leqslant \overline{\gamma}$, Eq. (2) thus predicts that the (fully budded) caveola shape is independent of membrane tension. In contrast, for $\gamma > \overline{\gamma}$ each value of $\beta_{\min}$ corresponds, for given L and C_0, to a unique value of γ.

For a constant line tension $\sigma > 0$ in Eq. (2), cuplike caveola shapes tend to be ruled out by a sharp transition from $\beta_{\min} = 1$ to $\beta_{\min} = \beta^* < 1$ with increasing membrane tension. In particular, at a critical membrane tension γ^* caveola states with $\beta = 1$ and $\beta = \beta^*$ have equal energy (see the green dashed curve in Fig. 2), yielding a discontinuous transition in caveola shape from $\beta_{\min} = 1$ to $\beta = \beta^*$ with increasing membrane tension [see the dashed curves in Fig. 3(a)]. The value of γ^* and the magnitude of this discontinuous jump in caveola shape depend on the values of L, C_0, and σ. In particular, for a given L and σ such that $\gamma^* \geqslant 0$, a decrease in C_0 results in a smaller γ^* and a greater discontinuous jump length $1 - \beta^*$. As $C_0 \to 0$ with $\sigma > 0$, we recover the bistable system described in Ref. [5], which rules out cuplike caveola shapes. Indeed, if G_σ dominates over G_κ and $C_0 \to 0$ in Eq. (2) the only two stable caveola shapes correspond to $\beta \approx 0$ and 1 at large and small membrane tension, respectively [5]. In contrast, for small enough σ, the discontinuity in the dependence of caveola shape on γ disappears, yielding a continuous spectrum of stable cuplike caveola shapes.

Figure 3(a) shows that the sensitivity of the stable caveola shape to changes in membrane tension depends crucially on the size and spontaneous curvature of caveolae. For $0 < \beta_{\min} < 1$, we can quantify the tension sensitivity of the caveola shape by taking the derivative of $\beta_{\min}$ with respect to membrane tension [see the partially transparent curves and right axes in Fig. 3(a)]. For $\sigma = 0$, the maximum magnitude of the tension sensitivity, $\mathcal{S}_{\max}$, is obtained at $\gamma = \overline{\gamma}$ in Eq. (4) for $L \geqslant 4/C_0$ and at $\gamma = 0$ for $L < 4/C_0$. We find that, for $\sigma = 0$, $\mathcal{S}_{\max} = L/\kappa C_0$ for $L \geqslant 4/C_0$ and $\mathcal{S}_{\max} = L^4 C_0^2/64\kappa$ for $L < 4/C_0$ [see the stars along the right axes in Fig. 3(a)]. Thus, for $\sigma = 0$, $\mathcal{S}_{\max}$ increases with L and decreases with C_0 for $L \geqslant 4/C_0$, but increases with both L and C_0 for $L < 4/C_0$. In contrast, for a constant $\sigma > 0$ in Fig. 3(a), we find that $\mathcal{S}_{\max}$ increases (weakly) with L as well as C_0 for the parameter ranges relevant for caveolae.

IV. CAVEOLA-SHAPE-DEPENDENT LINE TENSION

As noted above, cup-shaped caveolae are expected to deform the surrounding membrane [25], leaving a membrane footprint. Such caveola-induced membrane shape deformations may incur an energy cost that depends on β. Most straightforwardly, membrane footprints with smaller curvatures may be more favorable from an energetic perspective, thus increasing the stability of caveola states with small β. This scenario corresponds to a composition of the membrane footprint with zero spontaneous curvature [45]. We phenomenologically account for such situations by allowing for $\sigma = \sigma_+(\beta)$ with $\sigma_+(\beta) = \beta\ k_BT/\text{nm}$. Alternatively, curvature-sensing or curvature-generating lipids or proteins may be enriched in the curved membrane footprint of caveolae, and thus assist caveola budding [46,47]. Such situations correspond to a caveola membrane footprint with nonzero spontaneous curvature. A simple phenomenological description of this scenario is obtained by setting $\sigma = \sigma_-(\beta)$ with $\sigma_-(\beta) = (1-\beta)\ k_BT/\text{nm}$. Effectively, with $\sigma = \sigma_-$, the tendency of a finite line tension $\sigma > 0$ to stabilize curved membrane domains [5,17,18] is thus further amplified.

In analogy to Fig. 3(a), Fig. 3(b) shows the energetically preferred caveola shape $\beta_{\min}$ as a function of membrane tension for different values of C_0 and L, using the β-dependent line tensions $\sigma_+(\beta)$ and $\sigma_-(\beta)$. We find that, compared to $\sigma = 1\ k_BT/\text{nm}$, σ_+ yields a sharper transition in caveola shape from $\beta = 1$ to $\beta < 1$ as the membrane tension is increased from zero, with this transition occurring at smaller values of γ (see the dashed curves in Fig. 3). This can be understood by noting that, compared to $\sigma = 1\ k_BT/\text{nm}$, σ_+ biases the caveola shape towards more flattened states and thus decreases the energy cost of caveola flattening. In contrast, σ_- yields a greater range of stable caveola shapes with $0 < \beta < 1$ than $\sigma = 1\ k_BT/\text{nm}$ as well as $\sigma = 0$ in Fig. 3 (see the solid curves in Fig. 3). This follows because σ_- maximally penalizes caveola shapes with $\beta = 0$, thus yielding a more gradual transition towards caveola states with $\beta = 0$ as the membrane tension is increased.

In contrast to the constant σ considered and σ_+ in Fig. 3, σ_- can yield stable cuplike caveola shapes even for $C_0 = 0$, in regimes with large enough L and small enough γ [see the black solid curve in the right panel of Fig. 3(b)]. This follows

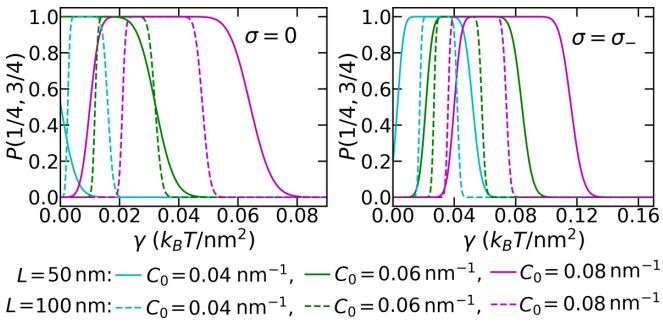

FIG. 4. Probability of caveola states with $1/4 \leqslant \beta \leqslant 3/4$, $P(1/4, 3/4)$ in Eq. (5) with the caveola energy in Eq. (2), as a function of membrane tension γ for $\sigma = 0$ (left panel) and $\sigma = \sigma_-(\beta) = (1-\beta)\ k_BT/\text{nm}$ (right panel) using $C_0 = 0.04$, 0.06, and 0.08 nm^{-1} at $L = 50$ nm (solid curves) and 100 nm (dashed curves). We set $\kappa = 20\ k_BT$.

because G_κ with $C_0 = 0$ favors flat caveola states while, as already noted above, σ_- progressively penalizes flatter caveola states compared to more budded caveola states. Finally we note that, depending on the values of C_0 and L considered, a dependence of σ on β can increase as well as decrease the tension sensitivity of the caveola shape [see the partially transparent curves in Figs. 3(b)]. We find that, for a given domain size and $C_0 > 0$, $\mathcal{S}_{\text{max}}$ increases with increasing C_0 for σ_- [see the stars along the right axes in Fig. 3(b)] and with decreasing C_0 for σ_+. For both σ_- and σ_+, larger $\mathcal{S}_{\text{max}}$ are obtained for larger L in Fig. 3(b).

V. CAVEOLA SHAPE DISTRIBUTION

Thermal fluctuations are expected to perturb the caveola shape about the energetically most favorable state $\beta = \beta_{\text{min}}$. A simple way to account for such thermal effects is to assume that the caveola shape is governed by a Boltzmann distribution. The probability of caveola states with $b_1 \leqslant \beta \leqslant b_2$ is then given by

$$P(b_1, b_2) = \frac{1}{Z}\int_{b_1}^{b_2} d\beta e^{-G/k_BT}, \tag{5}$$

where the normalization constant Z is chosen such that $P(0, 1) = 1$, G is given by Eq. (2), k_B is Boltzmann's constant, and T denotes the temperature of the system. We employ here Eq. (5) to predict the probability of finding cuplike caveola shapes and, in particular, focus on $b_1 = 1/4$ and $b_2 = 3/4$ in Eq. (5). We numerically evaluate $P(b_1, b_2)$ in Eq. (5) using PYTHON (version 2.7.12).

Figure 4 shows $P(1/4, 3/4)$ in Eq. (5) as a function of membrane tension for $\sigma = 0$ and $\sigma = \sigma_-$ in Eq. (2), respectively. We focus in Fig. 4 on these two choices for σ because the foregoing results show that a wide range of cuplike caveola shapes can be obtained with zero (or small) σ and σ that decrease with β. Furthermore, we focus in Fig. 4 on the range in spontaneous curvature $0.04 \lessapprox C_0 \lessapprox 0.08\ \text{nm}^{-1}$ most relevant for caveolae [1,2,10–13,33]. We find in Fig. 4 that, for $\sigma = 0$ as well as σ_-, larger values of C_0 and smaller values of L tend to yield a larger range in membrane tension for which caveola shapes with $1/4 \leqslant \beta \leqslant 3/4$ are dominant. For instance, for $\sigma = 0$ and $C_0 = 0.08\ \text{nm}^{-1}$ we find $P(1/4, 3/4) > 0.5$ in the membrane tension range $0.01 \lessapprox \gamma \lessapprox 0.07\ k_BT/\text{nm}^{-2}$ with $L = 50$ nm and $0.02 \lessapprox \gamma \lessapprox 0.05\ k_BT/\text{nm}^{-2}$ with $L = 100$ nm (see the solid and dashed purple curves in the left panel of Fig. 4). For $\sigma = \sigma_-$ and $C_0 = 0.08\ \text{nm}^{-1}$ we find $P(1/4, 3/4) > 0.5$ in the membrane tension range $0.04 \lessapprox \gamma \lessapprox 0.12\ k_BT/\text{nm}^{-2}$ with $L = 50$ nm and $0.04 \lessapprox \gamma \lessapprox 0.07\ k_BT/\text{nm}^{-2}$ with $L = 100$ nm (see the solid and dashed purple curves in the right panel of Fig. 4). Figure 4 illustrates that, within the ranges of C_0 and L relevant for caveolae, different values of C_0 and L tend to yield distinct caveola shapes in distinct membrane tension regimes. Combined with the results in Figs. 2 and 3, this suggests that cells may use heterogeneity in the values of C_0 and L to produce a staggered response of caveola shape to changes in membrane tension.

VI. CONCLUSION

We have explored here the roles of membrane bending, membrane tension, and the line tension of caveola domains [5,17,18] in stabilizing cuplike caveola shapes. We find that, for the range in membrane tension relevant for cell membranes [19–21], the competition between membrane tension and membrane bending yields caveolae with cuplike shapes similar to those observed experimentally [1,2,10–16], and that cuplike caveola shapes tend to be ruled out as the line tension of caveola domains comes to dominate the energy budget of caveolae. Our results suggest that the size and the spontaneous curvature of caveola domains are key control parameters for the stability of cup-shaped caveolae, and for the sensitivity of cup-shaped caveolae to changes in membrane tension. Heterogeneity in the size of caveola domains and heterogeneity in caveola spontaneous curvature due to, for instance, variations in the concentration of caveolin-1 in caveola domains, as well as spatial heterogeneity in membrane tension within cell membranes [21,48] or variations in the caveola line tension, may thus produce heterogeneity in caveola shape. Our calculations predict that variations in caveola shape yield heterogeneity in the response of caveolae to mechanical perturbations of the cell membrane, which may facilitate regulation of membrane tension over the wide range of scales thought to be relevant for cell membranes [19–21].

ACKNOWLEDGMENTS

This work was supported by NSF Grants No. PHY-1806381 (F.P. and C.A.H.) and No. DMR-1554716 (C.A.H.), and the James H. Zumberge Faculty Research and Innovation Fund at USC (C.A.H.).

[1] P. Nassoy and C. Lamaze, Trends Cell Biol. **22**, 381 (2012).
[2] R. G. Parton, Annu. Rev. Cell Dev. Biol. **34**, 111 (2018).
[3] R. G. Parton, K.-A. McMahon, and Y. Wu, Curr. Opin. Cell Biol. **65**, 8 (2020).

[4] P. Sens and M. S. Turner, in *Lipid Rafts and Caveolae: From Membrane Biophysics to Cell Biology*, edited by C. J. Fielding (Wiley, New York, 2006), Chap. 2, pp. 25–44.

[5] P. Sens and M. S. Turner, Phys. Rev. E **73**, 031918 (2006).

[6] R. G. Parton and K. Simons, Nat. Rev. Mol. Cell Biol. **8**, 185 (2007).

[7] B. Sinha, D. Köster, R. Ruez, P. Gonnord, M. Bastiani, D. Abankwa, R. V. Stan, G. Butler-Browne, B. Vedie, L. Johannes, N. Morone, R. G. Parton, G. Raposo, P. Sens, C. Lamaze, and P. Nassoy, Cell **144**, 402 (2011).

[8] S. Mayor, Cell **144**, 323 (2011).

[9] C. Morris and U. Homann, J. Membr. Biol. **179**, 79 (2001).

[10] R. G. Parton and M. A. del Pozo, Nat. Rev. Mol. Cell Biol. **14**, 98 (2013).

[11] T. Richter, M. Floetenmeyer, C. Ferguson, J. Galea, J. Goh, M. R. Lindsay, G. P. Morgan, B. J. Marsh, and R. G. Parton, Traffic **9**, 893 (2008).

[12] W. Schlörmann, F. Steiniger, W. Richter, R. Kaufmann, G. Hause, C. Lemke, and M. Westermann, Histochem. Cell Biol. **133**, 223 (2010).

[13] M. N. Lebbink, N. Jiménez, K. Vocking, L. H. Hekking, A. J. Verkleij, and J. A. Post, Traffic **11**, 138 (2010).

[14] A. Fernandez, M. Bautista, R. Stanciauskas, T. Chung, and F. Pinaud, ACS Appl. Mater. Interfaces **9**, 27575 (2017).

[15] M. Tachikawa, N. Morone, Y. Senju, T. Sugiura, K. Hanawa-Suetsugu, A. Mochizuki, and S. Suetsugu, Sci. Rep. **7**, 7794 (2017).

[16] I. M. Khater, Q. Liu, K. C. Chou, G. Hamarneh, and I. R. Nabi, Sci. Rep. **9**, 9888 (2019).

[17] R. Lipowsky, J. Phys. II France **2**, 1825 (1992).

[18] M. Zhang and A. Chen, Biomech. Model. Mechanobiol. **19**, 2657 (2020).

[19] R. Phillips, T. Ursell, P. Wiggins, and P. Sens, Nature (London) **459**, 379 (2009).

[20] Z. Shi and T. Baumgart, Nat. Commun. **6**, 5974 (2015).

[21] Z. Shi, Z. T. Graber, T. Baumgart, H. A. Stone, and A. E. Cohen, Cell **175**, 1769 (2018).

[22] S. Banerjee and M. C. Marchetti, New J. Phys. **15**, 035015 (2013).

[23] B. Hogan, A. Babataheri, Y. Hwang, A. I. Barakat, and J. Husson, Biophys. J. **109**, 209 (2015).

[24] E. W. Weisstein, Spherical Cap, from MathWorld—A Wolfram Web Resource, http://mathworld.wolfram.com/SphericalCap.html.

[25] G. Golani, N. Ariotti, R. G. Parton, and M. M. Kozlov, Dev. Cell **48**, 523 (2019).

[26] L. Pelkmans, T. Bürli, M. Zerial, and A. Helenius, Cell **118**, 767 (2004).

[27] M. M. Hill, M. Bastiani, R. Luetterforst, M. Kirkham, A. Kirkham, S. J. Nixon, P. Walser, D. Abankwa, V. M. Oorschot, S. Martin, J. F. Hancock, and R. G. Parton, Cell **132**, 113 (2008).

[28] T. Baumgart, S. T. Hess, and W. W. Webb, Nature (London) **425**, 821 (2003).

[29] P. B. Canham, J. Theor. Biol. **26**, 61 (1970).

[30] W. Helfrich, Z. Naturforsch. C **28**, 693 (1973).

[31] E. A. Evans, Biophys. J. **14**, 923 (1974).

[32] P. J. Walser, N. Ariotti, M. Howes, C. Ferguson, R. Webb, D. Schwudke, N. Leneva, K.-J. Cho, L. Cooper, J. Rae *et al.*, Cell **150**, 752 (2012).

[33] R. G. Parton, M. M. Kozlov, and N. Ariotti, J. Cell Biol. **219** (2020).

[34] F. Jülicher and R. Lipowsky, Phys. Rev. E **53**, 2670 (1996).

[35] F. Wong and A. Amir, Biophys. J. **116**, 2378 (2019).

[36] N. C. Gauthier, M. A. Fardin, P. Roca-Cusachs, and M. P. Sheetz, Proc. Natl. Acad. Sci. USA **108**, 14467 (2011).

[37] N. C. Gauthier, T. A. Masters, and M. P. Sheetz, Trends Cell Biol. **22**, 527 (2012).

[38] T. W. Hungerford, *Algebra* (Springer, New York, 1974).

[39] R. Sarasij, S. Mayor, and M. Rao, Biophys. J. **92**, 3140 (2007).

[40] H. Hägerstrand, V. Kralj-Iglič, M. Bobrowska-Hägerstrand, and A. Iglič, Bull. Math. Biol. **61**, 1019 (1999).

[41] N. S. Gov, Phil. Trans. R. Soc. B **373**, 20170115 (2018).

[42] M. Fošnarič, S. Penič, A. Iglič, V. Kralj-Iglič, M. Drab, and N. S. Gov, Soft Matter **15**, 5319 (2019).

[43] H. Alimohamadi, A. S. Smith, R. B. Nowak, V. M. Fowler, and P. Rangamani, PLoS Comput. Biol. **16**, e1007890 (2020).

[44] A. Iglič and H. Hägerstrand, Med. Biol. Eng. Comput. **37**, 125 (1999).

[45] L. Foret, Eur. Phys. J. E **37**, 42 (2014).

[46] M. Yáñez-Mó, P. R.-M. Siljander, Z. Andreu, A. B. Zavec, F. E. Borràs, E. I. Buzas, K. Buzas, E. Casal, F. Cappello, J. Carvalho *et al.*, J. Extracell. Vesicles **4**, 27066 (2015).

[47] L. Mesarec, M. Drab, S. Penič, V. Kralj-Iglič, and A. Iglič, Int. J. Mol. Sci. **22**, 2348 (2021).

[48] J. T. Groves, Dev. Cell **48**, 15 (2019).